Backgrounds and pulse shape discrimination in the ArDM liquid argon TPC

Journal of Cosmology and Astroparticle Physics
An IOP and SISSA journal

Backgrounds and pulse shape discrimination in the ArDM liquid argon TPC

The ArDM collaboration

J. Calvo,[a] C. Cantini,[a] P. Crivelli,[a] M. Daniel,[b] S. Di Luise,[a] A. Gendotti,[a] S. Horikawa,[a] L. Molina-Bueno,[a] B. Montes,[b] W. Mu,[a] S. Murphy,[a] G. Natterer,[a] K. Nguyen,[a] L. Periale,[a] Y. Quan,[a] B. Radics,[a] C. Regenfus,[a] L. Romero,[b] A. Rubbia,[a] R. Santorelli,[b] F. Sergiampietri,[a] T. Viant[a] and S. Wu[a]

[a]ETH Zurich, Institute for Particle Physics, Zurich, Switzerland
[b]CIEMAT, Div. de Física de Particulas, Avda. Complutense, 22, E-28040, Madrid, Spain

E-mail: andre.rubbia@cern.ch

Received January 23, 2018
Revised October 16, 2018
Accepted October 16, 2018
Published December 10, 2018

Abstract. The ArDM experiment completed a single-phase commissioning run (ArDM Run I) with an active liquid argon target of nearly one tonne in mass. The analysis of the data and comparison to predictions from full detector simulations allowed extraction of the detector properties and an assessment of the low background conditions. The ^{39}Ar specific activity from the employed atmospheric argon is measured to be (0.95±0.05) Bq/kg. The cosmic muon flux at the Canfranc underground site was determined to be in the range $(2\text{–}3.5)\times10^{-3}\,\mathrm{m^{-2}s^{-1}}$. The statistical rejection power for electronic recoil events using the pulse shape discrimination method was estimated using a ^{252}Cf neutron calibration source. Electronic and nuclear recoil band profiles were found to be well described by Gaussian distributions. Employing such a model we derive values for the electronic recoil statistical rejection power of more than 10^8 in the tonne-scale liquid argon target for events with more than 50 detected photons at a 50% acceptance for nuclear recoils. The ^{222}Rn emanation rate of the ArDM cryostat at room temperature was found to be (65.6±0.4) μHz/l. These results represent an important physics milestone for the next run in the double-phase mode and in the context of foreseen developments towards the use of depleted argon targets.

Keywords: dark matter detectors, dark matter experiments

ArXiv ePrint: 1712.01932

https://doi.org/10.1088/1475-7516/2018/12/011

JCAP12(2018)011

Contents

1 Introduction

ArDM is a direct dark matter detection experiment for Weakly Interacting Massive Particles (WIMPs) searches based on a liquid argon (LAr) target [1]. The detector system consists of a cylindrical Time Projection Chamber (TPC) containing LAr target mass of about 850 kg. The experiment is designed to detect signals produced by nuclear recoils (NR), and from background particles like β or γ producing electronic recoils (ER).

In 2015, a series of commissioning runs with gaseous or liquid argon targets have been performed in single-phase mode to explore the functionality and performance of the detector. The detector was operated stably during a long run in single phase called ArDM Run I. A detailed description of the setup and of the run can be found in ref. [2]. The different background sources have been studied and compared with a specially developed Monte-Carlo (MC) simulation. At low energy (below 1 MeV), the background is dominated by ^{39}Ar-β decays (Q value $\sim$565 keV), radioactive contaminants in the materials of the detector components, and from external γ sources. At medium energy (1–5 MeV), the background originates from Rn and its progeny, emanated from the small contamination of ^{238}U and ^{232}Th in the detector materials. In addition, at high energy ($>$ 5 MeV) the detector also recorded cosmic muon events.

The time structure of LAr scintillation is strongly correlated with the nature of the interaction, which provides a pulse shape discrimination (PSD) method, to reject the ER background events [3–6]. Analyzing data taken with a ^{252}Cf calibration source, the band profiles of ER or NR events were found to be well described by Gaussian distributions. Using

JCAP12(2018)011

the separation between the ER and NR bands, the capability of the PSD method to reject ER events is demonstrated.

For the longer term future with the goal to discover the nature of WIMP particles, it is important for direct detection experiments to improve current reaches by a several orders of magnitude. The ability to build experiments able to operate in a background-free mode is crucial. In this spirit, the four world-leading argon dark matter projects (ArDM, DarkSide-50, DEAP-3600 and MiniCLEAN) agreed on joining forces [7] to carry out a unified program for dark matter direct detection with ^{39}Ar depleted liquid argon, in the framework of the DarkSide-20k (DS-20k) project [8]. The natural ^{39}Ar depletion factor in gas extracted from the CO_2 wells at Cortez, Colorado, showed a residual ^{39}Ar specific activity of $(0.73 \pm 0.11) \times 10^{-3}$ Bq/kg [9] to be e.g. compared to the activity in atmospheric argon of to be (0.95±0.05) Bq/kg reported in this paper. It is not known and not proven that the reduction factor will be the same for all samples of gas extracted from underground wells, as local rock conditions can significantly alter the composition. Therefore, all future batches of underground argon will have to be tested individually. Plans are being developed to exploit the ArDM low background detector infrastructure for this task. The demonstration of the low background conditions of the ArDM setup and its ability to make sensitive measurements of low-level of ^{39}Ar contamination is therefore of crucial importance.

This paper mainly describes ArDM Run I data and its agreement with predictions from full detector simulations, and is organised as follows. Section 2 gives a brief general overview over the experimental concept of ArDM and the data taking period of Run I. In section 3 the electron like background is discussed using the comparison between the data and Monte-Carlo simulations of different radioactive isotopes, resulting in the measurement of the ^{39}Ar activity (section 4). In section 5 we present a measurement of ^{222}Rn emanation using data taken with GAr target at room temperature. Section 6 discusses cosmic muon rates observed in the data. The PSD method and the statistical rejection power results are presented in section 7. Section 8 gives an estimate on the sensitivity of the ArDM setup for a measurement of the ^{39}Ar content in the target. Finally, the work is concluded in section 9.

2 The ArDM experiment

The Argon Dark Matter (ArDM) experiment is located at the Spanish underground site LSC (Laboratorio Subterráneo de Canfranc) [10]. It is designed as a tonne-scale dual-phase liquid-argon time projection chamber (LAr TPC) to detect ionisation and scintillation produced by the recoiling nucleus in the argon medium [1]. The LAr TPC consists of 24 low-radioactivity cryogenic 8" PMTs distributed in two equal arrays for light readout, the top PMT array above the LAr target in the gaseous phase and the bottom array immersed in LAr [11, 12]. Nuclear recoils or electronic recoils in the argon medium generate scintillation light (S1) and electron-ion pairs. When the detector works in the dual-phase (liquid and gaseous) mode, the electrons can be separated from their ions in an electric field and drift upwards to the argon surface. After being extracted from the LAr to the gaseous argon (GAr) on top, these electrons are accelerated and the secondary scintillation light (S2), which is proportional to the amount of electrons extracted, is produced. Both S1 and S2, which are vacuum ultraviolet (VUV) light with a wavelength around 128 nm, can be wavelength shifted to visible range by a layer of tetraphenylbutadiene (TPB) deposited on the inner surfaces and read out by the PMT arrays. In the single-phase Run I with zero drift field, only S1 signals were recorded. More details about the experimental setup during Run I are reported in ref. [2].

JCAP12(2018)011

Run stage	**Recorded events [10^6]**
Warm gas	213
Cool-down	20
Cold gas	351
LAr filling	495
Full LAr target	
Open shield	1286
Closed shield	2025
Subtotal	**3310**
Warm-up & warm gas	308
Total	**4697**

Table 1. Summary of the number of recorded events at different stages of ArDM Run I.

Source	^{83m}Kr	^{57}Co	^{252}Cf	^{60}Co	^{22}Na	Total
Recorded events [10^6]	201	89	48	6	6	350

Table 2. Number of events recorded with calibration sources in the full LAr target during ArDM Run I.

Table 1 summarises the Run-I data recorded at different stages of the operation. The detector was commissioned first with a gaseous argon (GAr) target at room temperature, hereafter called warm gas. Then it was cooled down and was operated with a GAr target at LAr temperature, 87 K (cold gas). These were succeeded by the filling of the ArDM cryostat with a total of ∼2 tonnes of LAr. The detector was then operated over six months in the full target mode.

The detector vessel is surrounded by an equilateral octagonal polyethylene shield, where the top-cap (50 cm thick PE blocks) is a pre-assembled unit which can be removed by crane. Initially the top part of the polyethylene (PE) neutron shield, entirely surrounding the detector vessel, was left open (open-shield configuration) to allow accesses to various service ports located on the top cover of the vessel. When the stable performance of the detector had been achieved, the shield was closed (closed-shield configuration), resulting in a reduction of γ backgrounds originating from the external environment. After 3.3 billion triggers had been recorded with the full target, the liquid was evaporated slowly and the cryostat was warmed up. A total of 4.7 billion triggers have been recorded over the period of Run I. About 10% of this total data was collected during calibration runs with radioactive test sources. Metastable ^{83m}Kr atoms, which were injected into the gaseous phase and then diluted in the LAr target, served as a main source for the light yield calibration, along with an external ^{57}Co source. Likewise a ^{252}Cf neutron source was deployed to study the PSD capability, as reported below in section 7. The calibration data collected with the full LAr target is summarized in table 2.

3 Analysis of the electronic recoil background

The understanding of the β or γ induced ER background events is crucial in a low-energy experiment looking for nuclear recoils. We report in this section the selection of such events in data and their comparison to background simulations.

JCAP12(2018)011

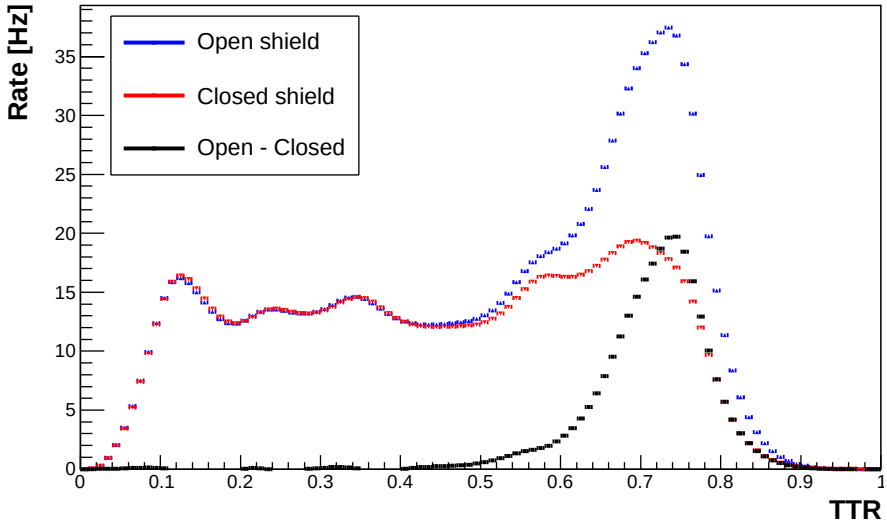

Figure 1. TTR distribution during data taken with open (blue), closed (red) top shield configurations. The difference of the two distributions is shown in black. TTR values larger than 0.5 correspond to vertical positions closer to the top of the detector.

3.1 Data selection

The energy deposited in an event is derived from the total detected light expressed in units of photo-electrons (pe). The total light of an event is calculated by finding and summing clusters of photon signals over the data acquisition time window of 4 μs. The light signals, $L_{\rm top}$ and $L_{\rm btm}$, are calculated from the sum of all signal clusters found in the top and the bottom PMTs, respectively. The total detected light $L_{\rm tot}$ is calculated from the sum of the signal from both PMT arrays. The light yield per keV electronic-equivalent energy deposit ($\rm keV_{ee}$) was calibrated using ^{83m}Kr and ^{57}Co sources. The obtained light yield in LAr was 1.1 $pe/$ keV with an error of 5% dominated by systematics (see [2] for details). A linear response over the entire energy range was found in agreement to other observations [13].

The pulse shape discrimination parameter $f90$ is defined as the ratio of the light detected in the first 90 ns of the event to the total detected light. This value is used to separate between ER and NR events. In addition, events with extreme $f90$ values ($f90 > 0.99$ or $f90 < 0.01$) are removed since they are not compatible with argon scintillation (mostly PMT dark counts). A sample of clear ER events can be identified by selecting events with $f90 < 0.6$.

The ratio of the light detected by the top PMT array to the total detected light, called top-to-total ratio TTR,

$$TTR \equiv L_{\rm top}/L_{\rm tot} = L_{\rm top}/(L_{\rm top} + L_{\rm btm}) \tag{3.1}$$

is used as a discriminator to select events along the vertical position (Z-axis in the ArDM coordinate system) in the LAr volume. Figure 1 shows the distribution of TTR values in the data after selection cuts in the open-shield and closed-shield configurations. The data sets are normalised for equal detector life time. Larger TTR values correspond to vertices closer to the top of the detector, and more light is collected in the top array. Values of about 0.1 and 0.8 correspond to events separated by about 1.3 m, in the very bottom or top (liquid level) of the LAr target, respectively. A main feature of the TTR distribution is an accumulation of events in the upper part of the detector in the shield open configuration, which allows to determine the external background. The accumulation at the top of the argon volume shows the self shielding action of the argon.

JCAP12(2018)011

3.2 ArDM simulation code

A Geant4 [14] based full simulation framework, including light ray-tracing, has been developed for ArDM. Details on the MC simulation program are reported in ref. [15]. The software contains a detailed geometric description of the internal detector components, as well as the surrounding structure with the passive PE neutron shield [2]. Material properties of the main detector parts, i.e. their contamination with radioactive traces, are estimated from screening campaigns [2]. The response of the ArDM detector is modelled from first principles starting by the production of argon VUV scintillation light in the target, up to the detection of visible photons in the PMT arrays. The Geant4 scintillation and wavelength-shifting processes were modified to describe the strength and time structures of VUV emission for the different event types (electronic and nuclear recoils), as well as the shifting of 128 nm light to a wavelength range around 420 nm by the thin TPB layers on the inner detector surfaces. Light propagation (e.g. VUV attenuation and Rayleigh scattering) in the LAr medium, as well as the reflection and refraction across different materials are implemented in function of the wavelength. The PMT response to (visible) photons, i.e. the production of photo-electrons, the signal response and amplitude fluctuations, were parameterised from laboratory measurements. Finally simulated events include digitised waveforms of the 24 PMT channels to reproduce the same format as the front-end electronics and DAQ. This allowed to reconstruct simulation events by the same software package as used for experimental data.

Several optical properties of materials could not be determined with high precision in the laboratory before the commissioning of the detector. Details of the optical processes were determined from data by tuning a set of parameters in the Monte-Carlo model. The light yield spectra of ER events as well as their TTR distributions (eq. (3.1)) were used for this purpose. The comparison of data to Monte-Carlo was done with ^{39}Ar β-events, as well as with ^{83m}Kr de-excitations from a calibration source ($\sim$42 keV). Two parameters were found to be most crucial for a correct description of the optics, the reflectivity $\mathcal{R}$ of the main reflector foil, as well as the attenuation length λ_{VUV} for VUV scintillation photons in the LAr bulk. The relatively low value, close to 0.5 m, was found for λ_{VUV} and was interpreted as a presence of optically active impurities in the liquid argon. Overall the MC simulation reproduced well the response of the detector. This is reported in more details in ref. [15].

Due to a relatively short mean free paths in liquid argon compared to the size of the target (6–20 cm for γ energies 200–2600 keV) most of the interaction vertices from γ background events occur near the edges of the argon volume (self-shielding effect). From simulations, more than 80% of the γ events contain two or more interaction vertices (Compton scatters). Multiple scatter γ events cannot be individually resolved. The mean distance of the multiple interaction points to the space point which is reconstructed from the (mean) TTR value is in the range of 6–9 cm depending on the energy.

3.3 Backgrounds simulation

We have produced MC simulations of γ background events from both internal and external sources, as well as for β background events from ^{39}Ar decay. ER events observed in the data are well described by a combination of three distinct components: (1) ^{39}Ar β-decays, (2) external and (3) internal γ sources. The β-electrons from ^{39}Ar were generated according to the theoretical spectrum described by the phase space factors, the Fermi correction, as well as the first forbidden Gamow-Teller transitions [15]. The γ backgrounds originate from environmental sources around the experiment at the underground site (external source) and in radioactive contamination of detector components (internal source). The radioactivity of

JCAP12(2018)011

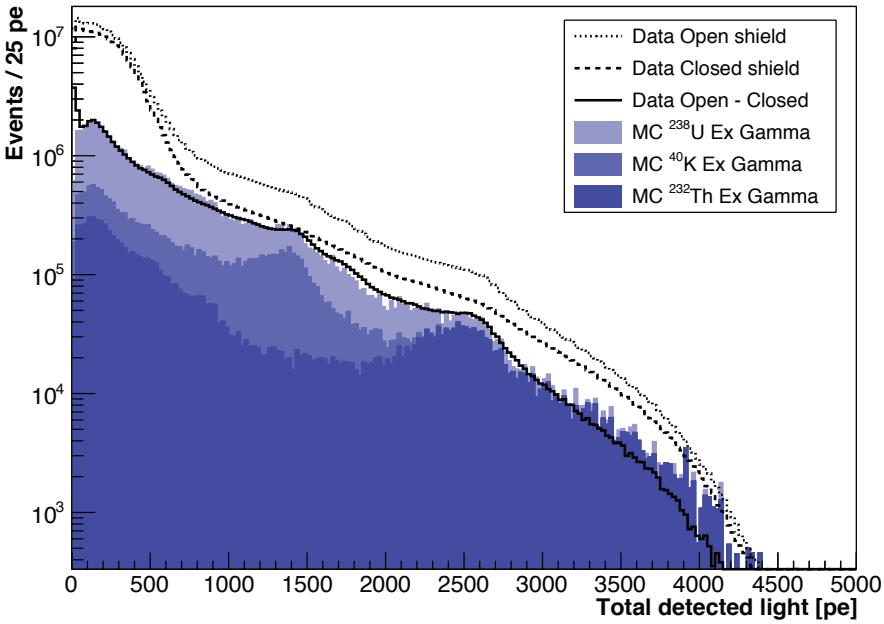

Figure 2. The comparison between the external γ background MC simulation (MC ^{238}U, ^{232}Th and ^{40}K) and data using the difference of light spectra obtained from data (solid line) taken with open (dotted line) and closed (dashed line) top shield detector configurations.

the detector components was determined in several material screening campaigns, using the high-purity germanium (HPGe) detector facility at LSC. Characteristic γ lines from different nuclei were identified and the corresponding activities were estimated. Main contributions to the γ activities were found to originate in the ^{238}U and ^{232}Th series, and additionally in ^{40}K or ^{60}Co. The ^{238}U and ^{232}Th decay chains are assumed to be in secular equilibrium. The detailed results are presented in ref. [2]. To simulate internal γ backgrounds, we assume a homogeneous distribution of radioactive isotopes inside the material of the corresponding detector components. For the external backgrounds, decays of radioactive isotopes are simulated uniformly on an envelope surrounding the PE neutron shield.

The external γ flux is extracted from the data by means of the difference in the TTR distribution of the measured ER spectra in the open and closed top-cap configurations. The spectra of the total detected light for open and closed shield configurations are shown in a semi-logarithmic representation in figure 2, together with the difference spectrum (solid line). The latter is well described by a combination of γ spectra obtained from the isotopes of the ^{238}U, ^{232}Th, and ^{40}K radioactive series. The number of events in the Monte-Carlo spectrum for the source of the isotope chain i ($i = {}^{238}$U, ^{232}Th, ^{40}K) is given as $N_{\mathrm{MC}i} = f_i \cdot N_{\gamma i} \cdot \epsilon_i$, where f_i is the scaling factor obtained from a fit to the difference of open and close shield light spectra from the data, $N_{\gamma i}$ the average number of generated γ photons in the simulation and ϵ_i the event acceptance, as determined by the simulation. The equivalent external γ flux $j_{\gamma i}$ originating from the source i can then be obtained as

$$j_{\gamma i} = \frac{f_i \cdot N_{\gamma i}}{2 \cdot t_{\mathrm{D}} \cdot A} \; [\mathrm{cm}^{-2}\mathrm{s}^{-1}], \tag{3.2}$$

where t_{D} [s] is the live time for the data taking. The external γ fluxes were normalized to 0.72 ± 0.4, 0.13 ± 0.02 and $0.05 \pm 0.02\,\mathrm{cm}^{-2}\,\mathrm{s}^{-1}$ for ^{238}U, ^{232}Th and ^{40}K respectively.

JCAP12(2018)011

3.4 Electronic recoil background fit

The ^{39}Ar background, the internal backgrounds and the external ones are fit to the data using the Bayesian Analysis Toolkit (BAT) [16]. The MC template based binned likelihood model is a linear sum of the simulation samples obtained for the various radioactive isotopes in the total light spectrum. The model assumes Gaussian uncertainties in each bin of the spectrum. Given the data, BAT finds the best parameters in the template likelihood model by numerically evaluating the Bayes theorem, varying the parameters of the template model, and calculating various credibility intervals from the full posterior distribution. The model parameters are the individual relative contributions of each Monte-Carlo sample and the light yield scale. This latter parameter was introduced to allow for uncertainties in the light yield calibration in the data. Less than ∼5% variation was sufficient to describe any possible light scale uncertainty. The following model was used for the parametrization of the prediction of the total light spectrum in the data from Monte-Carlo simulations, $f_{\mathrm{MC}}(x)$,

$$f_{\mathrm{MC}}(x) = p_0 \cdot g^{^{39}\mathrm{Ar}}(x') + p_1 \cdot g_{\mathrm{Ex}}^{^{238}\mathrm{U}}(x') + p_2 \cdot g_{\mathrm{Ex}}^{^{232}\mathrm{Th}}(x') + p_3 \cdot g_{\mathrm{Ex}}^{^{40}\mathrm{K}}(x') + \sum_i \sum_j p_{ij} \cdot g_{\mathrm{Int}}^{ij}(x') \tag{3.3}$$

where x denotes the light signal bin, $g^{\psi}(x')$ is the binned MC template likelihood for the ψ component with a corresponding scale parameter p_{ψ}, in the double sum, i and j indexes run through the isotope chains and the detector components, respectively, and $x' = x - p \cdot x$ allows for light scale variation between the data and MC simulations. The BAT framework performs the numerical evaluation of the Bayes-theorem, given some data D, $p(\vec{a}|\vec{D}) = p(\vec{D}|\vec{a})p(\vec{a})/p(\vec{D})$ where $p(\vec{a}|\vec{D})$ denotes the conditional probability of a given parameter set, $\vec{a}$ (which are the individual scaling factors for the various radioactive isotopes and detector components, etc), given the dataset $\vec{D}$, $p(\vec{D}|\vec{a})$ denotes the conditional probability of the dataset given the parameter set, and finally $p(\vec{a})$ and $p(\vec{D})$ denote the probability of the parameter set and that of the data, respectively. The conditional probability is evaluated as a Gaussian Likelihood

$$p(\vec{D}|\vec{a}) = \prod_i \frac{1}{\sqrt{2\pi}\sigma} e^{-\frac{(y_i - f(x_i;\vec{a}))^2}{2\sigma^2}} \tag{3.4}$$

where y_i is the number of events detected in bin i, and i runs through each bin of the total light signal distribution. During the evaluation flat priors were used, with loose parameter boundaries given by the flux results obtained from the external γ difference spectrum and from material screening results. During the BAT evaluation strong correlations were not found between the parameters.

Figure 3 shows the spectrum of the total detected light for ER events in data (black dots) compared to Monte-Carlo simulations (filled coloured histograms) with scaling parameters for each component obtained from the best values from the BAT fit. A data sample of ∼ 150 million events was selected requiring $0.4 < TTR < 0.6$ and $0.0 < f90 < 0.6$. This cuts selects events of roughly 20% of the central part of the LAr target which is the most sensitive to internal background contributions.

Good agreement is obtained between data and predictions, showing that all relevant sources of events are accounted for. The computed rates of the various background sources is shown in table 3. The dominant component is ^{39}Ar-β decays, amounting to ∼74% of the selected events, is consistent with the expected value of ∼1 Bq/kg. The remaining contributions are compatible with events originating from internal and external sources, amounting

JCAP12(2018)011

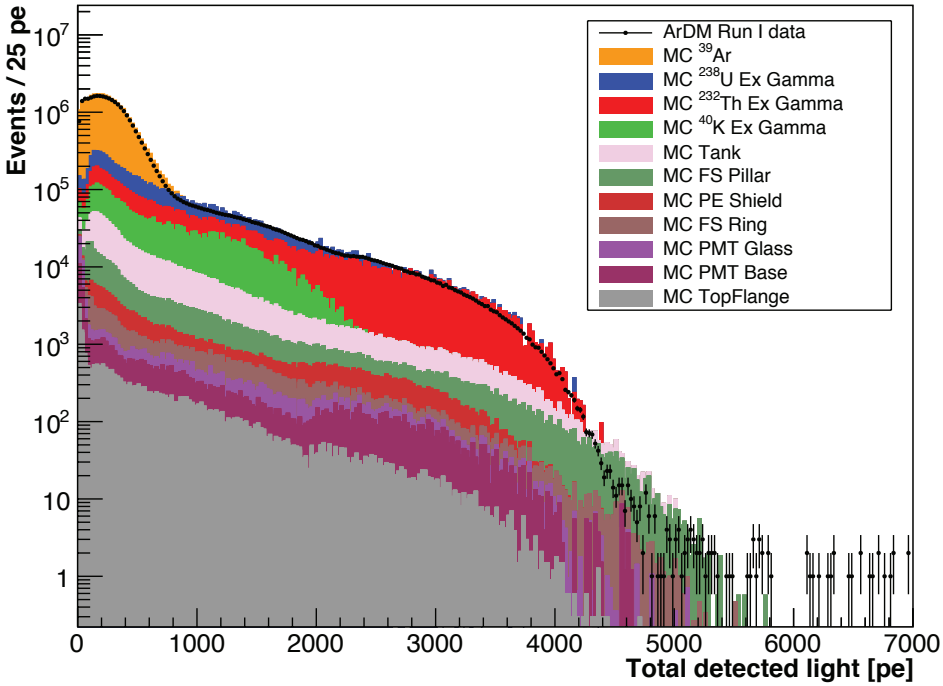

Figure 3. Comparison of the experimentally obtained ER light spectrum to various backgrounds derived from the MC simulations. The events are selected using $0.4 < TTR < 0.6$ and $0 < f90 < 0.6$.

to ∼22% and ∼4% of the events, respectively. The uncertainties around the rates have been estimated by allowing a variation in the background contributions by 50% and repeating the Bayesian evaluation. The ^{238}U contribution was found to have the largest relative uncertainty, however, overall it only presents a ∼25% error in the total external gamma rate. The estimated uncertainty on the total rate from Monte-Carlo simulation is at a level of ∼7%.

4 Results on the ^{39}Ar specific activity of atmospheric argon

The ^{39}Ar specific activity $\mathcal{A}$ can be determined from the model evaluation results presented in the previous section, using $N_{^{39}\mathrm{Ar}} = t_{\mathrm{D}} \cdot \epsilon \cdot m \cdot \mathcal{A}$, where $N_{^{39}\mathrm{Ar}}$ is the number of detected ^{39}Ar events, t_{D} is the live time of the data taking, ϵ is the event acceptance determined from the MC simulation, and m is the argon mass. The measured ^{39}Ar specific activity of atmospheric argon is

$$\mathcal{A} = (0.95 \pm 0.05)\ \mathrm{Bq/kg} \tag{4.1}$$

The measurement uncertainties come from the fiducial volume estimation and the extracted fraction of ^{39}Ar events from the analysis. This result is consistent with the WARP measurement [17].

5 Results on ^{222}Rn emanation

Recoils produced by α particles from ^{222}Rn and its progeny can mimic signals expected from WIMP interactions, if their energy is only partially detected. In order to estimate the contamination, we study ^{222}Rn emanation in the detector at room temperature using data taken with a GAr target. This can be considered as an upper limit due to the higher

JCAP12(2018)011

Component	Rate [Hz]
^{39}Ar	219±4
External ^{238}U	27±16
External ^{232}Th	22±3
External ^{40}K	17±8
Tank	6.6±2.9
Fieldshaper pillar	2.0±0.9
Polyethylene shield	0.6±0.3
Fieldshaper ring	0.4±0.2
PMT glass	0.3±0.1
PMT base	0.3±0.1
Top Flange	0.2±0.1
Total MC	295 ±19
Total data	274

Table 3. Electronic recoil background composition in the Monte-Carlo model. The events are selected using $0.4 < TTR < 0.6$ and $0 < f90 < 0.6$.

temperature where ^{222}Rn (generated from the ^{238}U chain) is diffusing out faster from the materials and does not attach to cold surfaces. The measurement was done with a fresh fill of argon gas of the ArDM target looking for increase of the signal rate with a time constant of 3.82 day, the half-life of ^{222}Rn.

The signals from internal ^{222}Rn and its progeny are monitored by counting the decays of the isotopes ^{222}Rn, ^{218}Po, and ^{214}Po in the energy region between 5 and 7 MeV, and the 5.49 MeV α signals from the decay of ^{222}Rn are used to measure the emanation rate of ^{222}Rn. In order to identify the 5.49 MeV α events originating from the bulk of the gas, a fixed energy window is used together with a TTR discrimination, $0.32 < TTR < 0.64$, corresponding to 217.0±5.7 liters of fiducial volume. To avoid the collisional quenching effect of argon triplet excimers due to the impurities present in GAr, we use detected light in the fast component between 500 and 800 pe to select ^{222}Rn events.

Figure 4 shows the ^{222}Rn event rate variation after the detector tank was pumped and refilled with pure GAr. The red curve is an exponential fit to the data. During the fit the half-life was fixed to be 3.82 days according to the literature value. The ^{222}Rn emanation rate increased exponentially, but not from zero. This indicates that the ^{222}Rn atoms emanate from both the detector materials and the gas bottle. We set an upper limit for the emanation rate of ^{222}Rn atom as 65.6±0.4 μHz/l for the ArDM detector.

6 Estimation of crossing muons rate

To estimate the rate of muons crossing the detector, a total number of 1.27×10^9 events are preselected requiring $0.26 < f90 < 0.55$. Their reconstructed energy is shown in a double logarithmic scale in figure 5, spanning eight orders of magnitudes. At low energies the spectrum is dominated by ^{39}Ar β events ($< 10^3\,pe$), while the middle energy part is dominated by radiogenic γ backgrounds, described in the previous sections. We interpret the events above the relatively sharp cut-off around $4\times10^3\,pe$ as been induced by cosmic rays

JCAP12(2018)011

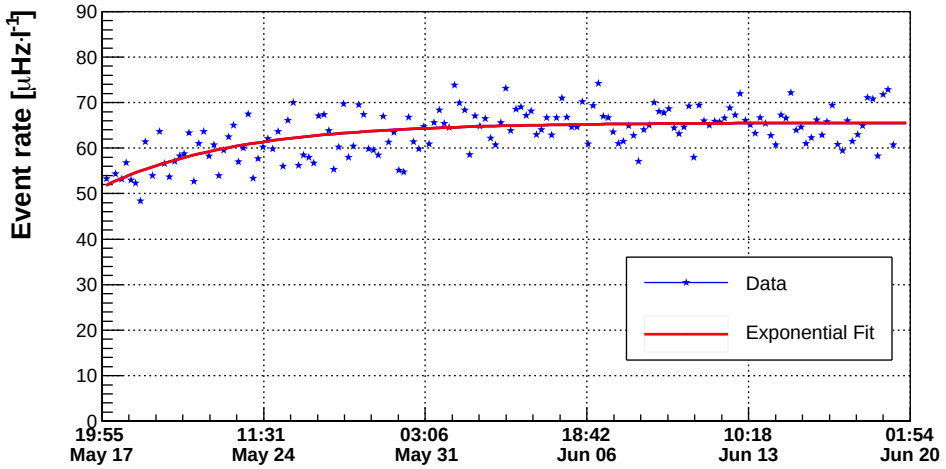

Figure 4. The ^{222}Rn rate as a function of time during data taking with room temperature GAr target. The red curve is an exponential fit to the data, $R(t) = A - B \times e^{-t/\tau}$, where the parameter τ is fixed to $\tau_{1/2} = 3.82$ days.

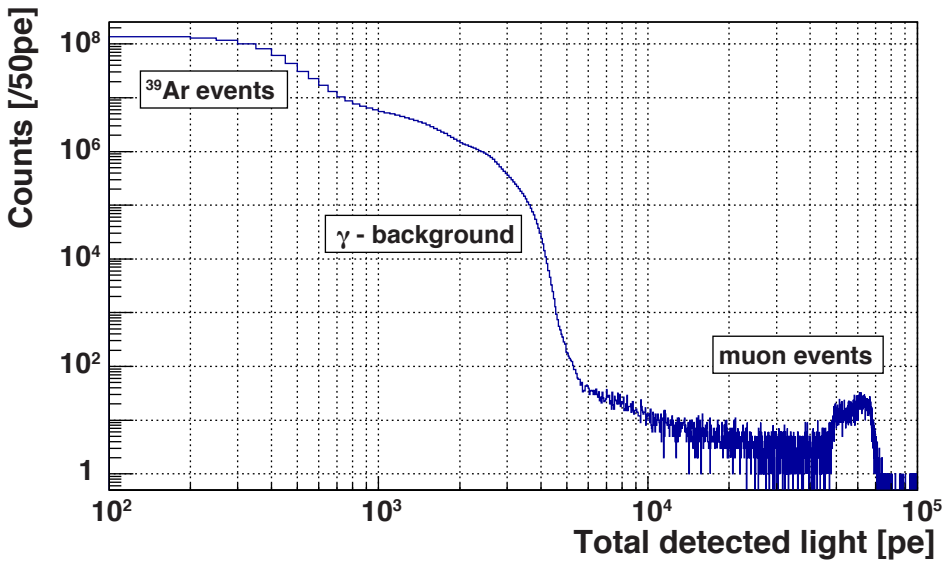

Figure 5. Distribution of total light in pe in double logarithmic scale. Different class of events are indicated. Cross-muons accumulate at the highest values.

partially or fully crossing the argon volume. The tail and peak features in this part of the spectrum correspond to showers in the rock.

From the life-time of the detector during the recording of this data (1.18×10^6 s, 13.6 days) and the amount of events under the main peak (7445) we find a cosmic muon rate in Hall A of LSC of $2.1\times10^{-3}\,\mathrm{m^{-2}\,s^{-1}}$, by assuming an effective area of $3\,\mathrm{m^2}$ of the ArDM LAr target. The muon events in the tail at high energy corresponds to a rate of $3.5\times10^{-3}\,\mathrm{m^{-2}\,s^{-1}}$, consistent with the value $(2\text{–}4)\times10^{-3}\,\mathrm{m^{-2}\,s^{-1}}$ from ref. [18].

JCAP12(2018)011

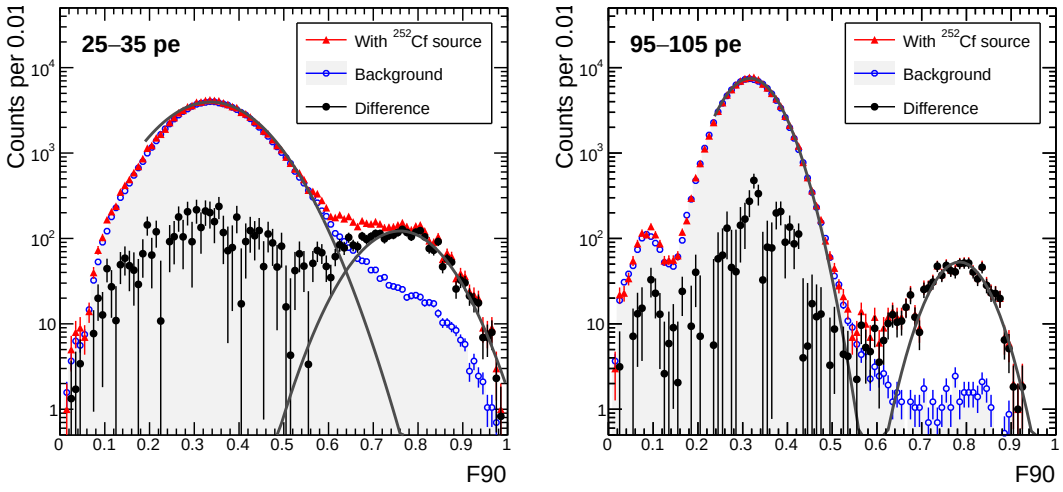

Figure 6. Gaussian fit to $f90$-histograms for selected energy bins of 25–35 pe (left) and 95–105 pe (right). The figure shows the data with the ^{252}Cf source (red triangles), the background data taken without the ^{252}Cf source (blue dots) and the difference the two dataset (black dots). The ER and NR band fit results are shown as solid, gray lines.

7 Electronic recoil statistical rejection power

An important property of LAr as a target is the capability to reject electronic recoil background processes at a very high level using pulse-shape discrimination [19]. The classification of events into ER and NR-type allows to quantify the rejection capability in the large target volume of ArDM. The statistical rejection power for ER events is evaluated by calculating the leakage of events from ER ($0.2 < f90 < 0.6$) into the NR region ($0.7 < f90 < 1.0$). The ER contamination ($\mathcal{ERC}$) is defined as the probability of incorrectly classifying an ER event as a NR event given a particular level of NR acceptance. The PSD rejection power ($\mathcal{REJ}$) is then calculated from the tail integral of the ER Gaussian function around the NR region, as follows,

$$\begin{cases} \mathcal{ERC}(N) = \dfrac{\int_{M_{\rm nr}-N\cdot\sigma_{\rm nr}}^{M_{\rm nr}+3\cdot\sigma_{\rm nr}} G_{\rm er}(M_{\rm er},\sigma_{\rm er})}{\int_{0.0}^{M_{\rm nr}+3\cdot\sigma_{\rm nr}} G_{\rm er}(M_{\rm er},\sigma_{\rm er})} \\ \mathcal{REJ}(N) = \dfrac{1}{\mathcal{ERC}(N)} \end{cases} \tag{7.1}$$

Here N is the measure of the amount NR acceptance, expressed in Gaussian sigma units distance from the mean, $M_{\rm nr}$, of the Gaussian approximated NR event distribution, $M_{\rm er}$ and $\sigma_{\rm er}$ are the mean and sigma of the Gaussian functions, $G_{\rm er}(M_{\rm er},\sigma_{\rm er})$, fitted to the data in the ER region.

We use a dataset of 23.8×10^6 events collected with ^{252}Cf calibration source placed around the detector. The $f90$ distributions are constructed in various total light bins between 15 and 205 pe. Figure 6 shows the $f90$ distribution for two energy ranges: 25–35 pe and 95–105 pe. The ^{252}Cf source data is the red triangles, the background data taken without the ^{252}Cf source are the blue dots and the difference the two dataset is plotted with black dots. The Gaussian functions in the ER region are fitted in the range $0.2 < f90 < 0.6$. In order to increase the signal-over-background ratio in the NR region we first subtract the background (dominated by ER events from ^{39}Ar-β decays and the external γ photons) from

JCAP12(2018)011

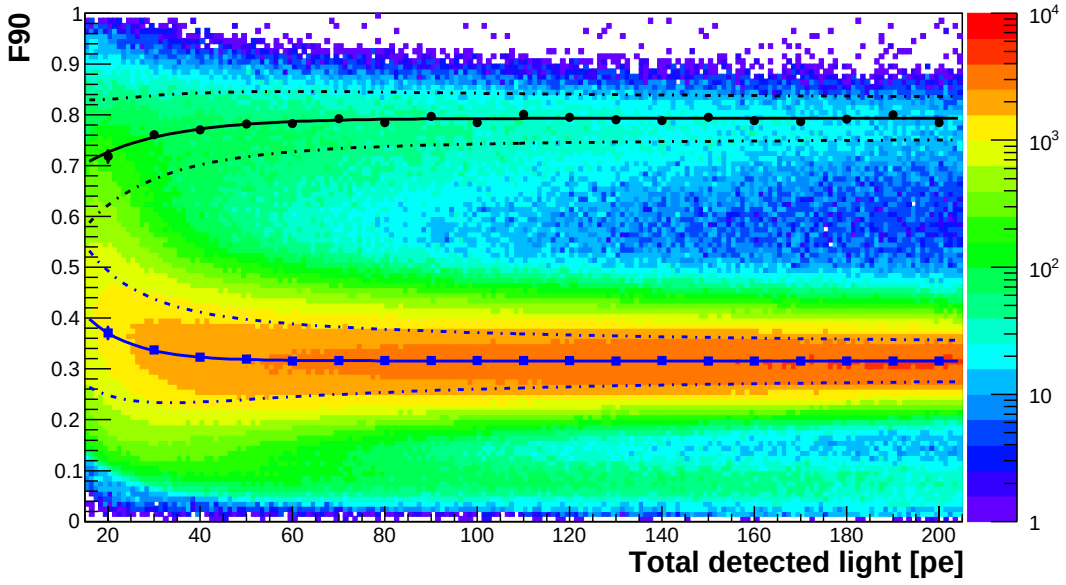

Figure 7. $f90$ vs total detected light using ^{252}Cf data. The black dots and blue squares show the $f90$ mean values for NR and ER events of each energy slice, respectively. The black and blue solid lines are the fitted parametrisations for the $f90$ mean values for NR and ER events, respectively. The black and blue dashed lines cover the $1\,\sigma$ region around the obtained $f90$ mean values.

the $f90$ distributions and fit the Gaussian functions to each residual histogram in the range $0.7 < f90 < 1.0$. The result of the fitting procedure is also illustrated in figure 6 as solid, gray lines. We parameterise the obtained $f90$ Gaussian mean values ($M_{\rm er}$, $M_{\rm nr}$), as a function the total light, with exponential functions. In a similar way, the $f90$ Gaussian σ-values ($\sigma_{\rm er}$,$\sigma_{\rm nr}$) are parameterised with a function of the form $\sigma(L_{\rm tot}) = A + B/(L_{\rm tot} - C)$. The fit results together with the parameterised mean and sigma values are shown in figure 7.

The ER statistical rejection power is calculated from the parameterised values using eq. (7.1). The results are shown in figure 8 as a function of the light signal for 50%, 84.0%, 97.6%, and 99.7% NR acceptance levels, corresponding to [0, $3\sigma_{\rm nr}$], [-$\sigma_{\rm nr}$, $3\sigma_{\rm nr}$], [-$2\sigma_{\rm nr}$, $3\sigma_{\rm nr}$], and [-$3\sigma_{\rm nr}$, $3\sigma_{\rm nr}$] limits across the calculated NR mean value $M_{\rm nr}$. As an example, for a 50% NR acceptance level, the PSD rejection power is larger than 10^8 for events with total detected light larger than $50\,pe$, corresponding to about $50\,{\rm keV_{ee}}$ using the observed light yield.

8 Sensitivity to detect ^{39}Ar decays in depleted argon

The DS-20k project plans to use ^{39}Ar depleted argon as target to reach zero background conditions. One of the important milestone is the provision of several tens of tons of depleted argon, collected from well gases [8]. Thanks to the large target mass and the low background conditions, the ArDM facility at LSC is well suited to determine the depletion factor for low ^{39}Ar argon of future batches to be produced in view of DS-20k.

The sensitivity to the ^{39}Ar β-decay activity can be derived from the measurements obtained in this paper. The simulated interaction vertices of γ photons in the LAr target are plotted in figure 9 (left) as a function of the vertical (Z) and the radial (R) coordinate. Contributions from all the simulated internal and external sources were scaled according to the measurements. Thanks to the self-shielding of the large LAr target, a clear accumulation of the events near the edges of the active volume is visible.

JCAP12(2018)011

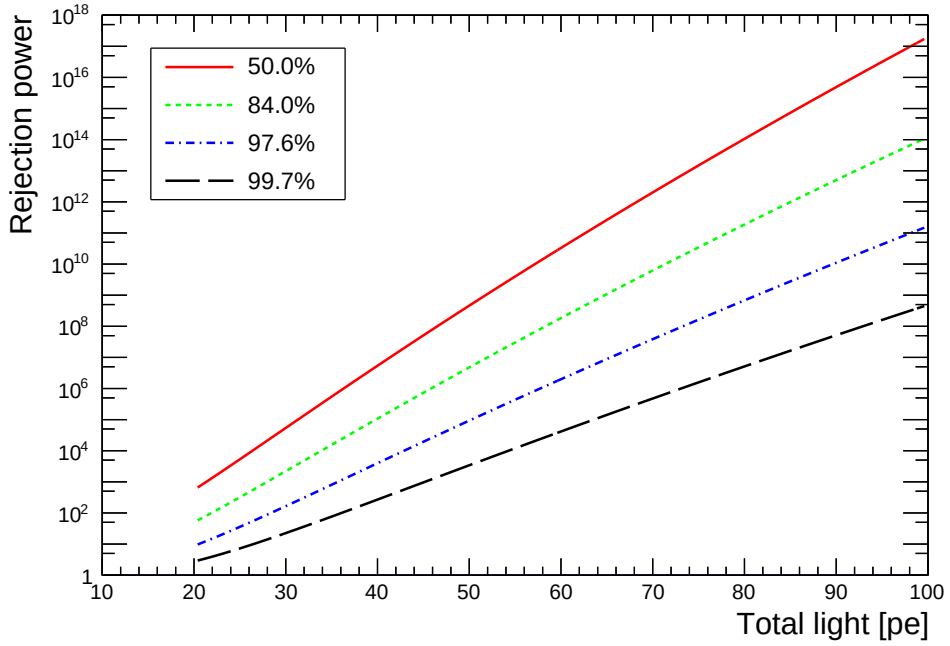

Figure 8. The measured ER PSD rejection power for different NR events acceptance rates as a function of the detected number of photons.

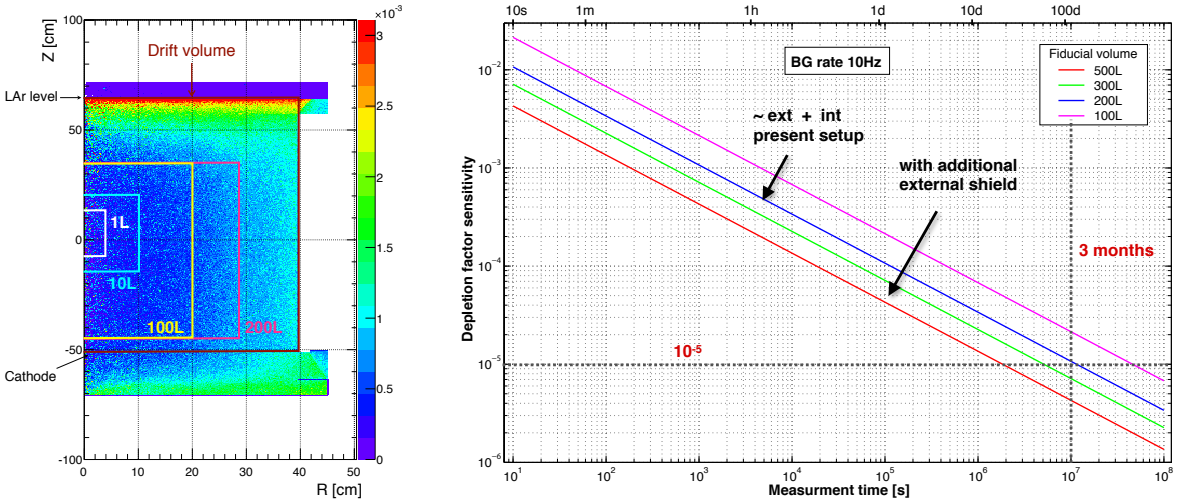

Figure 9. Left: simulated interaction vertices of the internal and external γ backgrounds in the LAr target, plotted as a function of the vertical (Z) and the radial (R) coordinate. The boxes show the four different fiducial volumes under study, as well as the active drift volume of the ArDM TPC. Right: 3σ sensitivity to the ^{39}Ar depletion factor at a given measurement time in ArDM.

Four different fiducial volumes depicted in figure 9 (left), were investigated. An S2 threshold of 2 keV for the energy deposit at each vertex was applied. The resulting rates of the γ background for the four fiducialisations are summarised in table 4 with the rejection rate. The rates were calculated by the integral of the reconstructed light spectra in the range of the ^{39}Ar β-spectrum, 50–600 *pe*.

JCAP12(2018)011

FV	Total γ Bkg in FV [Hz]	Rejected [Hz]	Remaining Bkg [Hz]	Rejection rate
200 ℓ	32.7	21.6	11.1	66.0%
100 ℓ	11.3	9.5	1.8	84.5%
10 ℓ	1.26	1.20	0.06	95.6%
1 ℓ	0.164	0.160	0.004	97.3%

Table 4. Simulated γ background (Bkg) rates for four different fiducial volumes (FV) with and without event rejection based on the vertex reconstruction using S2 signals. The rates were calculated by the integral of the reconstructed light spectra (see figure 3) in the range 50–600 *pe*.

Figure 9 (right) shows the sensitivity of ArDM towards the ^{39}Ar content in the target. The numbers are calculated for a 3σ measurement of the event rate in the ^{39}Ar β-spectrum over statistical background fluctuations. These estimates indicate, that a measurement time of a few weeks would be needed to determine depletion factors up to 10^5 in respect to atmospheric argon, which is within the requirements for DS-20k.

9 Conclusion

In this paper measurement results have been presented on backgrounds and pulse shape discrimination of the ArDM experiment using Run I data. From the Monte-Carlo model fitted to the data the ER background at low energy is found to be dominated by events originating from ^{39}Ar-β decays, which contribute to the selected events at level of $\sim$ 74%. The specific activity of ^{39}Ar has been estimated to be $\sim$ 1Bq/kg, consistent with measurements in the literature. In the 1–4 MeV energy range the external γ background dominates with an overall contribution of $\sim$ 22% and the internal detector components contribute at a level of $\sim$ 4%. The external γ background flux has been measured, using the light spectrum difference between open and closed top shield configurations, and the total flux is estimated to be 0.9 $\mathrm{cm}^{-2}\,\mathrm{s}^{-1}$. From these measurements, the low background conditions of the ArDM setup have been assessed.

At medium and high energies, signals produced by ^{222}Rn and cosmic muons contribute to the data. From the data taken with GAr target at room temperature we estimate the ^{222}Rn emanation rate to be 65.6$\pm$0.4 μHz/l, which shows that the radon level was low during ArDM Run I. From the ER light spectrum at high energy, the cosmic muon flux is estimated to be in the range (2.1–3.5) $\times 10^{-3}$ $\mathrm{m}^{-2}\,\mathrm{s}^{-1}$.

Using the pulse shape discrimination method the ER statistical rejection power is found to be more than 10^8 at 50% NR acceptance and more than 50 *pe* detected. Together with recent results reported by DEAP-3600 [20], this study shows the excellent performance obtainable with liquid Argon targets at the tonne scale.

Finally, the measured low levels of background demonstrate that it will be possible to use this experimental facility in order to measure the depletion level of future batches of liquid argon foreseen to be used in the next generation DS-20k experiment.

Acknowledgments

We acknowledge the support of the Swiss National Science Foundation (SNF) and the ETH Zurich, as well as the Spanish Ministry of Economy and Competitiveness (MINECO) through the grants FPA2012-30811 and FPA2015-70657P.

JCAP12(2018)011

We thank the directorate and the personnel of the Spanish underground laboratory *Laboratorio Subterráneo de Canfranc* (LSC) for the support of the ArDM experiment. We also thank CERN for continued support of ArDM as the CERN Recognized RE18 project, where part of the R&D and data analysis were conducted.

References

[1] A. Rubbia, *ArDM: A Ton-scale liquid Argon experiment for direct detection of dark matter in the universe*, *J. Phys. Conf. Ser.* **39** (2006) 129 [hep-ph/0510320] [INSPIRE].

[2] ArDM collaboration, J. Calvo et al., *Commissioning of the ArDM experiment at the Canfranc underground laboratory: first steps towards a tonne-scale liquid argon time projection chamber for Dark Matter searches*, *JCAP* **03** (2017) 003 [arXiv:1612.06375] [INSPIRE].

[3] M.G. Boulay and A. Hime, *Technique for direct detection of weakly interacting massive particles using scintillation time discrimination in liquid argon*, *Astropart. Phys.* **25** (2006) 179 [INSPIRE].

[4] P. Benetti et al., *First results from a Dark Matter search with liquid Argon at 87 K in the Gran Sasso Underground Laboratory*, *Astropart. Phys.* **28** (2008) 495 [astro-ph/0701286] [INSPIRE].

[5] DarkSide collaboration, P. Agnes et al., *First Results from the DarkSide-50 Dark Matter Experiment at Laboratori Nazionali del Gran Sasso*, *Phys. Lett.* **B 743** (2015) 456 [arXiv:1410.0653] [INSPIRE].

[6] DEAP collaboration, P.A. Amaudruz et al., *Measurement of the scintillation time spectra and pulse-shape discrimination of low-energy β and nuclear recoils in liquid argon with DEAP-1*, *Astropart. Phys.* **85** (2016) 1 [arXiv:0904.2930] [INSPIRE].

[7] M. Battaglieri et al., *US Cosmic Visions: New Ideas in Dark Matter 2017: Community Report*, arXiv:1707.04591 [INSPIRE].

[8] C.E. Aalseth et al., *DarkSide-20k: A 20 tonne two-phase LAr TPC for direct dark matter detection at LNGS*, *Eur. Phys. J. Plus* **133** (2018) 131 [arXiv:1707.08145] [INSPIRE].

[9] DarkSide collaboration, P. Agnes et al., *Results From the First Use of Low Radioactivity Argon in a Dark Matter Search*, *Phys. Rev.* **D 93** (2016) 081101 [arXiv:1510.00702] [INSPIRE].

[10] A. Badertscher et al., *ArDM: first results from underground commissioning*, 2013 *JINST* **8** C09005 [arXiv:1309.3992] [INSPIRE].

[11] ArDM collaboration, C. Amsler et al., *First results on light readout from the 1-ton ArDM liquid argon detector for dark matter searches*, 2010 *JINST* **5** P11003 [arXiv:1009.3641] [INSPIRE].

[12] ArDM collaboration, A. Marchionni et al., *ArDM: a ton-scale LAr detector for direct Dark Matter searches*, *J. Phys. Conf. Ser.* **308** (2011) 012006 [arXiv:1012.5967] [INSPIRE].

[13] DarkSide collaboration, T. Alexander et al., *Light Yield in DarkSide-10: A Prototype Two-Phase Argon TPC for Dark Matter Searches*, *Astropart. Phys.* **49** (2013) 44 [arXiv:1204.6218] [INSPIRE].

[14] GEANT4 collaboration, S. Agostinelli et al., *GEANT4: A Simulation toolkit*, *Nucl. Instrum. Meth.* **A 506** (2003) 250 [INSPIRE].

[15] ArDM collaboration, J. Calvo et al., *Measurement of the attenuation length of argon scintillation light in the ArDM LAr TPC*, *Astropart. Phys.* **97** (2018) 186 [arXiv:1611.02481] [INSPIRE].

[16] A. Caldwell, D. Kollar and K. Kröninger, *BAT: The Bayesian Analysis Toolkit*, *Comput. Phys. Commun.* **180** (2009) 2197 [arXiv:0808.2552] [INSPIRE].

JCAP12(2018)011

[17] WARP collaboration, P. Benetti et al., *Measurement of the specific activity of ar-39 in natural argon*, *Nucl. Instrum. Meth.* **A 574** (2007) 83 [astro-ph/0603131] [INSPIRE].

[18] A. Bettini, *The Canfranc Underground Laboratory (LSC)*, *Eur. Phys. J. Plus* **127** (2012) 112 [INSPIRE].

[19] M.G. Boulay and A. Hime, *Direct WIMP detection using scintillation time discrimination in liquid argon*, astro-ph/0411358 [INSPIRE].

[20] DEAP-3600 collaboration, P.A. Amaudruz et al., *First results from the DEAP-3600 dark matter search with argon at SNOLAB*, *Phys. Rev. Lett.* **121** (2018) 071801 [arXiv:1707.08042] [INSPIRE].

JCAP12(2018)011